ORIGINAL PAPER

Measuring the impact: new insights into flood-borne large wood collisions with river structures using an isolated sensor-unit

Gabriel Spreitzer[1,2] · Diego Ravazzolo[2,3] · Jon Tunnicliffe[4] · Heide Friedrich[2]

Abstract

Large Wood (LW) transported during floods or channelized mass flows poses a high risk for engineered structures, often leading to significant damage or total failure of the impacted structure. To date little is known about impact magnitudes caused by LW collisions. To better control for such interactions, a better understanding of transport dynamics and impact forces is required. The present laboratory study employs state-of-the-art sensor units installed in scaled logs to capture acceleration data from collisions of waterborne LW with 2 in-stream structures—bridge pier and retention structure—each providing different examples of rigid engineered systems. Through precise measurements of acceleration and impact duration (stopping time), the resultant impact forces of LW collisions can be calculated. Here, for the first time, impact forces were quantified in a scaled stream environment based on the inertial frame of the object causing the impact, rather than the more commonly used instrumented structure approach. High-resolution accelerometer measurements were compared to conventional analytical (force balance) approaches. They revealed the need for accurate inertia measurements to appropriately account for prevailing hydraulic flow conditions and the effects of LW interactions in fluvial environments. Although log velocity and stopping time are crucial parameters for assessing LW impact forces, accurate measurements are still elusive due to limitations in available sensing techniques. By presenting proof-of-concept results, this study contributes to an improved understanding of LW impact forces during floods. Based on these encouraging results, we recommend more sensor-based field studies in future, needed for the design of resilient structures.

Keywords Large wood (LW) · Impact forces · Instream wood dynamics · Sensor-tagged LW · Physical modeling

---

✉ Gabriel Spreitzer
spreitzer@vaw.baug.ethz.ch

Extended author information available on the last page of the article

1 Introduction

1.1 Large wood in fluvial systems

Large wood (LW) plays an important role in fluvial systems. While at rest in the channel, wooden elements are known for enhancing river ecosystems (Gurnell et al. 2002), by augmenting natural sediment storage (Keller et al. 1979), regulating flow (Gippel 1995), and offering shelter and food supply for riverine organisms (Fausch and Northcote 1992). In general, LW is defined as wood pieces with lengths longer than 1 m and a diameter greater than 0.1 m (Nakamura and Swanson 1994; Abbe and Montgomery 2003; Wohl and Jaeger 2009; Martin et al. 2018). Despite the benefits of wood in rivers at low flow conditions, LW is often observed to negatively affect channel hydraulics, bed topography, river infrastructure, and human populations in adjacent areas during floods (Mazzorana and Fuchs 2010; Gasser et al. 2019). Studies that have focused on LW dynamics in rivers (Iroumé et al. 2015; Ravazzolo et al. 2015; Ruiz-Villanueva et al. 2019; Ghaffarian et al. 2020) have reported safety concerns, as LW abundance can pose a dire hazard to engineered structures in fluvial environments, such as bridges, weirs but also buildings in flooded areas (Asghar et al. 2020, Marvi 2020). LW thus poses a considerable hazard during floods.

1.2 Large wood dynamics (mobilisation, transport and deposition)

LW is typically mobilized whilst flow depth is increasing during the rising limb of the hydrograph (Ravazzolo et al. 2015). Most LW has been found to follow a trajectory along the thalweg of single-thread channels with parallel alignment to the flow (Braudrick and Grant 2001). However, interactions of individual wooden elements with the flow and other LW pieces (congested transport) or banks and in-channel bars, may disturb parallel and centered movement, adding more complexity to transport dynamics (Ruiz-Villanueva et al. 2016), and generating more random, unstable paths for wood moving in a flood. The use of active and passive remote frequency identification (RFID) tags and commercial GPS trackers installed into logs (MacVicar et al. 2009; Schenk et al. 2014; Ravazzolo et al. 2015; Wyżga et al. 2017), as well as video monitoring of LW transport (MacVicar and Piégay 2012; Ruiz-Villanueva et al. 2019; Ghaffarian et al. 2020), have improved the understanding of wood dynamics (e.g., log mobilisation, transport, and deposition), travel distance and velocities. Recent studies have estimated LW velocity from video footage of debris flows (Ravazzolo et al. 2017; Ruiz-Villanueva et al. 2019), from which important knowledge about LW dynamics has been gained.

The techniques that have been employed thus far have typically proven unable to capture a continuous record of LW location, orientation, and velocity. The observer must deduce these measures by interpolating along the stream section's defined start and end position. This results in the estimation of linear transit routes, as well as averaged log velocities across the stream study sections, which cannot satisfactorily account for interactions of LW with the flow (e.g., transiting through changing hydraulic conditions such as flow deflections, eddies, or secondary flow fields), and thus the problem remains unexplored to date. A new generation of mobile, embedded (isolated) sensor technologies is promising tool for developing an improved understanding of the physical kinetics (e.g., acceleration, velocity) of LW interactions. Over the past few years, new high-precision, miniature yet robust sensing platforms have emerged, with significant potential for application in LW research.

A recently introduced sensing method by Spreitzer et al. (2019) used a multi-degree of freedom (9-DoF) sensor (comprising an accelerometer, gyroscope, and magnetometer), implanted into scaled wooden dowels—SmartWood—which showed high potential for the capture of inflow LW dynamics, including complex interactions with turbulent flow and in-stream structures. With the research community's growing interest in the determination of LW's capacity for erosion and impact in rivers (Shields and Alonso 2012), precise and calibrated measurements of such impacts have become an important priority.

1.3 Estimation of impact forces in fluvial environments

There have been numerous reports of damage to bridge piers, bridge decks, and flood-plain structures arising from LW impacts (Haehnel and Daly 2004; Elliot et al. 2012; Wohl et al. 2016; Sturm et al. 2018). Although significant advances have been made in exploring impact magnitudes on structures resulting from tsunamis (Ko et al. 2015; Goseberg et al. 2016; Chuang et al. 2020; Stolle et al. 2020) and debris loaded flows (Jakob et al. 2011; Eu et al. 2019; Nam et al. 2019), little knowledge is available about LW impacts in fluvial environments. With the approximation of log mass based on wood density, Gilbert and Murphy (1914) and Braudrick et al. (1997) developed a physical framework for assessing the linkages between LW orientation, momentum, and force delivered to obstacles along the channel. Other studies have applied single-degree-of-freedom (1-DoF) models for estimating the impact forces of tsunami debris elements and vessels (AASHTO 1998; Haehnel and Daly 2004; Ikeno et al. 2016). Since then, several approaches have emerged to calculate the maximum impact magnitude of collisions in fluvial environments (Haehnel and Daly 2004).

Parameters such as impact duration, stopping distance, as well as stiffness of materials and impacted structures are used to estimate impact forces. Vessels and shipping containers usually collide at low velocities, relative to their very large inertia, typically resulting in a long impact duration (Riggs et al. 2013; Piran Aghl et al. 2014). The impacts between floating ice and other large structures have similarly long-duration impacts (Sodhi and Haehnel 2003). On the other hand, logs, transported during floods, are assumed to strike within a fraction of a second, showing a relatively short impact duration. Given the typically high modulus of elasticity and large mass of the in-stream structure compared to the stiffer and smaller impacting log, the log rebounds from the in-stream structure before the structure experiences any appreciable motion. Although this is rather more similar to a vehicle colliding on a bridge pier, in terms of stiffness variations of materials, as well as relatively short impact durations (El-Tawil et al. 2005; Zhou et al. 2017), the mass of a car/truck is much lower than those of vessels or ice shields, thus impacts are generally occurring at a much higher velocity. Thus, the resulting impact forces are rather similar, with known magnitudes of 10^3–10^7 kN (Kamaitis 1995; Chung et al. 2013; Sha and Hao 2013; Zhou et al. 2019). By contrast, typical impact forces of prototype-scaled LW and similar-sized debris range between 10^2 and 10^4 N (Haehnel and Daly 2004; Ko et al. 2015; Ikeno et al. 2016; Stolle et al. 2018). LW impacts are often simulated via a 1-DoF rigid model, where a spring-mass-system accounts for the impact stiffness (Haehnel and Daly 2004). As an alternative to the rigid LW impact model, a more complex system can be applied, using a 2-DoF model and Hooke's Law to simulate a two-spring system (Fan and Yuan 2014; Liang et al. 2017; Stolle et al. 2019).

To determine the maximum impact force, either accurate measurements of LW acceleration are needed, or else a suite of measurements that include LW velocity, impact duration,

and a reasonably precise estimate of LW mass is required. Based on Newton's Second Law of motion—force is equal to the change in momentum per unit time—the impact force can then be directly calculated from sensor data. The acceleration term already contains impact duration. In general, three different approaches for the estimation of the maximum impact forces on a basis of LW velocity and weight can be distinguished: (i) the Impulse-Momentum approach, as presented by the Federal Emergency Management Agency (FEMA 1995), (ii) the Work-Kinetic Energy approach, as presented by the National Association of Australian State Road Authorities (NAASRA 1990), and (iii) the Contact-Stiffness approach, as presented by the American Association of State Highway and Transportation Officials (AASHTO 1998). The principal metric from these three approaches is expressed in one parameter: the impact duration for the Impulse-Momentum approach, the stopping distance for the Work-Kinetic Energy approach, and the effective contact stiffness of the impact for the Contact-Stiffness approach. However, each of these parameters relies on a time component. By obtaining a time series of the impact event (e.g., stopping time or impact duration), and then transforming the results according to the available and commonly applied approaches, impact forces may be estimated precisely.

Impact forces and the impact duration of debris may be measured with inertial measurement units (IMUs), providing a low-cost and highly effective remote sensing technology. These sensors originate from sports analysis and animal behavior analysis (Ahmad et al. 2013; Aldoumani et al. 2016). They have been applied across LW (Spreitzer et al. 2019) and tsunami research (Goseberg et al. 2016), offering novel insights into water-borne object movement dynamics and impact scenarios. Besides position and orientation estimates, using sensor fusion from accelerometer, gyroscope, and magnetometer data (Ahmad et al. 2013; Fischer et al. 2013), sensor data from accelerometers are particularly useful for studying impact forces. Major advances have been achieved in measuring impact forces using sensor units in the automotive industry, recording crash tests (Xu et al. 2018), and medicine (Worsey et al. 2019). For LW in motion, changes in acceleration continuously occur as a result of interactions with the flow, channel boundaries, engineered structures, and other LW elements. In providing acceleration and impact duration data, impact forces of LW in transit can be determined more accurately. Currently, there is a lack of data and knowledge about LW collisions and resulting dynamic forces, which are urgently needed to appropriately assess structural vulnerability and account for LW impact forces (Bein 1990; Stolle et al. 2019). The employment of IMUs in LW research creates an opportunity to measure impact duration as well as resulting forces from collisions more precisely.

1.4 Objectives and motivation

The present work aims to employ isolated high-resolution accelerometer data in a physical model study to capture relevant parameters (e.g., log orientation, deceleration, impact duration), enabling the quantification and evaluation of LW impact forces arising from collisions with rigid in-stream structures. Using a sensor-tagged miniature log, which is naturally entrained and transported by flood flows, acceleration and impact duration are captured upon collision with 2 sets of in-stream structures (bridge pier and retention mesh) for a range of flow rates. In addition to the 100 Hz time series data acquired from the accelerometer, conventional 30 Hz video footage of the experiments is recorded as a check on LW velocity and orientation during transport and impact. Critical details of LW dynamics can thus be determined from the high-resolution sensor data. The results obtained in the present study offer some novel insights into disparities between this new measurement

technique and conventionally calculated impact forces, under the consideration of prevailing hydraulic flow conditions at a bridge pier, and negligible hydraulic effects at a log retention structure.

The applied 'Langrangian perspective' and instrumentation offer strong potential for future field experiments and the characterization of load dynamics of transported debris during natural hazards. The sensor-based method and gained knowledge are of great relevance for LW research, investigating impact forces upon bridge piers, LW retention structures, and other engineered structures in the channel (e.g., weirs, tilt-elements, engineered log jams). Its applicability is extended to a range of other hazard related research areas, such as the investigation of transported debris during hyper-congested floods (Ruiz-Villanueva et al. 2019), landslides (Caviezel et al. 2019; Cabral et al. 2021) or tsunamis (Chuang et al. 2020). Overall, improved knowledge about impact forces will enable engineers to assess the vulnerability of existing structures, refine hazard and risk assessments, and help design new flood-resilient structures and buildings in hazard areas (Nadal et al. 2010, Marvi 2020).

2 Methodology

2.1 Laboratory setup

A series of flume experiments was conducted at the Water Engineering Laboratory of the University of Auckland. A 6.3 m long and 1.5 m wide flume was used for the LW impact studies. The experimental setup was scaled at a ratio of 1:15, accounting for geometries, kinematics, and dynamics in the flume. A fixed meandering stream channel was laid out, based on a typical New Zealand headwater gravel-bed stream planform morphology, with rough channel elements (e.g., bars, rock ledge), and a constricted section (bridge with pier) at a distance of 4 m downstream from the inlet (Fig. 1). The fixed lateral channel boundaries were covered with an 8–16 mm grain mixture cemented in place. The experimental channel had near-bank full conditions, with a bed slope of 0.02 m m^{-1}. The water surface profile was maintained with a tailgate at the outlet section. Flume runs used mobile gravel bed conditions (4–63 mm); a sediment trap was installed at the outlet to collect time-integrated yield from experiments. The inlet flume pump could deliver flow rates of up to 150 l s^{-1}, though flow rates for the experiments ranged between 10 and 75 l s^{-1}. Delivery of
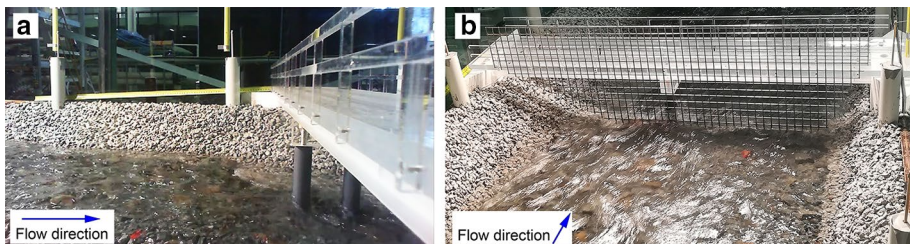

Fig. 1 Experimental setup for testing impact forces of LW on bridge piers **a**, and retention structures **b**. The retention structure is modeled by using a welded wire mesh obstruction (22 mm grid). The wire mesh obstruction did not affect flow behavior and the arrangement led to a higher number of straight impacts, in contrast to the mid-channel row of piers

sediment and wood near the inlet was regulated via a 3 m long and 0.5 m wide conveyor-belt system. The conveyor-belt system was set up to simulate the natural LW supply, with random orientation, from upstream.

2.2 Constricted cross-section (CCS)

The channel transitions through a constricted cross-section (CCS), flowing under a single-lane bridge with a central pier row (Fig. 1a). The model bridge is 1.5 m long ($L_P = 22.5$ m), 240 mm wide ($W_P = 3.6$ m), and crosses the channel bed at a height of 240 mm ($H_P = 3.6$ m). In the center of the channel, the bridge is supported by a central pier row with three cylindrical piers, each with a diameter of 36 mm ($D_P = 0.54$ m). The bridge pier and its effects on the flow play a key role in the present study. All elements of the bridge are made of polyvinyl chloride (PVC). 1 m upstream from the first bridge pier, a reference-line, consisting of red-colored gravel particles, was installed as a distance indicator for camera recordings.

In addition to impact studies on a bridge pier, the second set of experiments was conducted using a LW retention structure with negligible hydraulic effects on the flow. This setup included a welded wire mesh obstruction (22 mm grid), which was installed across the full cross-section at the upstream bridge pier and allowed for testing of impact forces at natural flow conditions (Fig. 1b) with no backwater effects. The wire mesh was suitably stiff ($d = 3.2$ mm), as required for simulation of a rigid system. There was no appreciable deformations or displacement of the structure (wire mesh) at dowel impact. A gap of 25 mm, measured from the mesh bottom to the channel bed, was maintained to allow for the transit of bedload material.

2.3 Sensor-tagged LW

An innovative sensor unit was used to measure the impact forces arising from collisions of LW with hydraulic structures under consideration of prevailing flow conditions. The IMU consists of an accelerometer, gyroscope, and magnetometer (e-compass), each measuring in 3-DoF, and a large battery (1.6 V, 600 mAh) for power supply. Furthermore, the custom-designed sensor unit contains an on-board memory card (2 MB), a processor for time-synchronization of sensor data, several programmed functions (e.g., wake-up, sleep, individual measurements) with adjustable threshold values, and Wi-Fi connection (915 MHz) for communication between sensor unit and computer, ranging up to 100 m. The sensor unit measured acceleration forces in a range of − 16 to + 16 g, at a resolution of 0.5 milli-g (mg). To attain high-resolution data, the measuring frequency was set to 100 Hz, entailing a maximum noise signal of 1.5 mg for accelerometer data, 0.04 deg s^{-1} rms (root mean square) gyroscope data, and about 2 µT for magnetometer data. Sensor data from the accelerometer also capture the Earth's gravitational acceleration. The sensor-unit used in this study underwent a thorough verification procedure, documented in Spreitzer et al. (2019), prior to the experiments. Battery life, as well as memory size, are sufficient to continuously record experiments.

The sensor-unit measures 105 mm in length and 10 mm in diameter, and was embedded into a cylindrical miniature log (SmartWood—Fig. 2), measuring 267 mm (length) by 22 mm (diameter), similar to dowels used by Braudrick and Grant (2001), Rusyda et al. (2014) and Gschnitzer et al. (2017). The experimental setup represents logs without branches and no root wad, such as commonly produced during harvesting operations
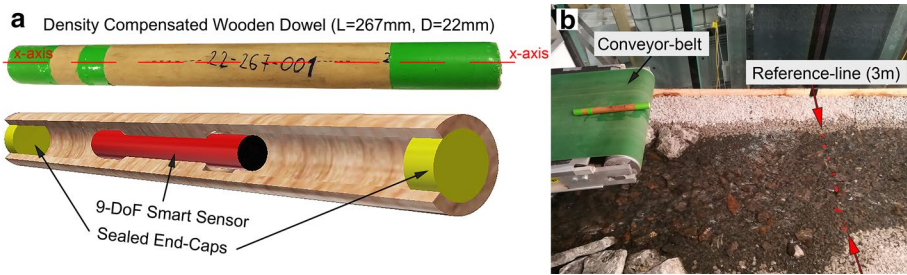
Fig. 2 Sensor-tagged wooden dowel (SmartWood) with a length of 267 mm and a diameter of 22 mm **a**. The sensor-tagged wooden dowel was fed into the channel via conveyor-belt system **b**, at a speed of 3 mm s^{-1}

in timber production and often found in stream channels (Cave et al. 2017; Phillips et al. 2018). To maintain natural and balanced transport (buoyancy) characteristics of the sensor-tagged wooden dowel, the sensor-unit must be installed in the center of gravity of the dowel while additionally requiring a density compensation, to account for the relatively heavy sensor-unit (~ 13.5 g), in comparison to the relatively light wooden dowel. Therefore, a 10 mm hole was drilled through the longitudinal centerline of the dowel, while larger holes (12 mm diameter, 80 mm length) at each end of the dowel were bored to further reduce weight. The design density of the sensor-tagged wooden dowel was set to 0.5 g cm^{-3}, in line with common practices of LW physical modeling (Braudrick and Grant 2000), resulting in a weight of 47.5 g for the sensor-tagged dowel in dry conditions. The actual weight of the wetted dowel, as used for the experiments, was measured as 50 g, which equals a prototype weight of roughly 170 kg, such as also applied previously (Haehnel and Daly 2004) for LW impact studies. The IMU is encased in waterproof housing. Yet, for additional protection of the sensor unit from water, the outermost ends (20 mm) of the dowels were filled with foam (polyurethane), and the caps were additionally sealed with a thin layer of hot-melt adhesive (ethylene–vinyl acetate), creating a stiff surface.

2.4 Video recording

All experiments were recorded using two video cameras—Microsoft Logitech webcam series—which were installed to capture (i) the reach immediately upstream of the CCS, showing the last meter of the sensor-tagged dowel in transit before impact, and (ii) the entire channel, with view from the flume inlet downstream. The cameras were operated simultaneously at a resolution of 854 × 480 pixels, with a frame rate of 30 frames per second (fps). As demonstrated in other studies (Ravazzolo et al. 2017; Ruiz-Villanueva et al. 2019), video footage is a good resource for wood monitoring research. Video footage of the experiments helps to verify dowel velocity estimates, and confirm the sensor data (e.g., impact orientation, dowel trajectory). Video analysis was performed in Pelscope (Codecian Co Ltd 2007), allowing for the extraction and analysis of individual frames from the video.

2.5 Experimental procedure

Prior to the experiments, the sensor-tagged dowel was soaked in water for 2 hours, assuring the miniature log's most realistic and consistent wetted condition throughout the

experimental tests. For each experimental test, the sensor-tagged dowel was placed upon the conveyor belt and fed into the channel at a constant speed of 3 mm s^{-1}, always ensuring the same initial orientation relative to flow direction. After positioning the dowel on the conveyor belt, the sensor was launched for data acquisition and the 2 cameras were started for video recording. The sensor-tagged dowel dropped over the front edge of the conveyor belt into the channel (0.5 m height), before being mobilized and transported by the flow. To enable realistic and consistent hydraulic flow conditions for testing impact forces of LW on in-stream structures, tests using three different flow rates (10, 35, and 75 l s^{-1}) were undertaken for each channel obstruction (bridge pier and wire mesh). For each flow rate and obstruction in the channel, 50 individual tests were conducted, resulting in 150 tests for each obstruction. The flow rates were controlled by an electromagnetic flow meter and valve, at a constant head elevation of 10 m. The flow rate of 10 l s^{-1} resulted in a flow depth of 40–45 mm along the main channel, ensuring a dowel diameter to flow depth ratio of 0.5; enough to mobilize and transport the sensor-tagged dowel downstream. Experiments were considered successful when the sensor-tagged dowel hit either the bridge pier or the wire mesh obstruction at 'straight' orientation (Fig. 3). Here, 'straight' impacts are defined as collisions of the sensor-tagged dowel with its longitudinal x-axis (Fig. 2a) aligned with the flow direction ($\pm30°$). Once the sensor-tagged dowel passed the bridge pier or accumulated at the wire mesh obstruction, sensor data acquisition was stopped, and memory was read.

2.6 Data analysis

The present study exclusively focuses on straight (head-on) impacts with a tolerance of $\pm30°$ from the longitudinal sensor axis to flow direction (Fig. 3). Sensor data from the accelerometer

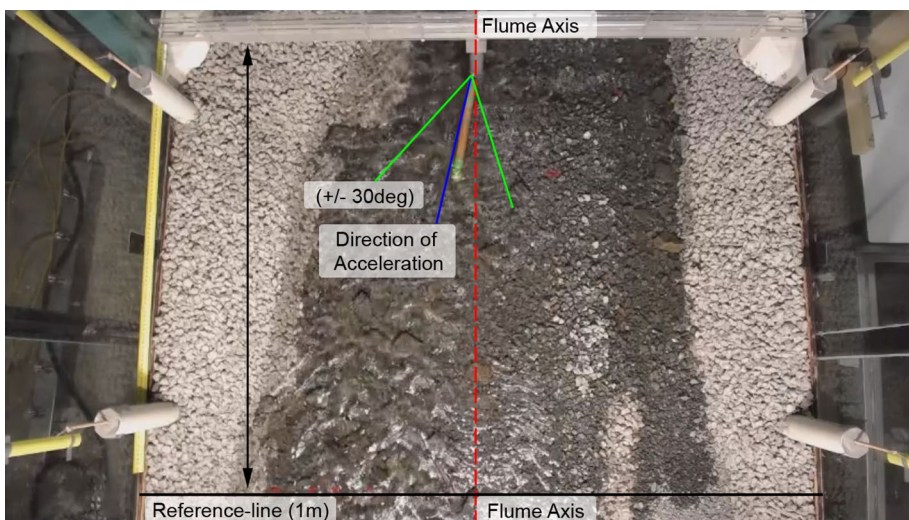**Fig. 3** Analysis of straight impact forces of the sensor-tagged wooden dowel on the bridge pier at a flow rate of 10 l s^{-1}. The analysis used a $\pm30°$ threshold in classifying 'straight impacts' from the direction of acceleration. A colored reference line (red), at a distance of 1 m upstream of the bridge pier, was used for the velocity estimation of the dowel

were analyzed for the peak magnitude during collisions with the bridge pier and the wire mesh. The sensor data also provided precise information about the impact duration (stopping time, which is defined as the time between the initial contact of the log with the in-stream structure and the peak magnitude of the impact FEMA 1995; U.S. Army Corps of Engineers 1995; Haehnel and Daly 2004).

Video footage from the camera, capturing the CCS (Fig. 3), was used for velocity estimates of the sensor-tagged miniature log. At 1 m upstream of the bridge pier, the red reference line was used as distance measure and represented the starting point of the velocity tracking range. As soon as the front end of the sensor-tagged dowel passed the reference line, it was tracked frame by frame until initial contact with the structure (impact). The mean dowel velocity was then estimated from the distance traveled (1 m) over time. Initial available information thus includes (i) acceleration and timing, from the accelerometer, (ii) mean velocity of the sensor-tagged wooden dowel over the last meter before impact, and (iii) the wetted weight (50 g) of the sensor-tagged wooden dowel. Based on these data, the impact magnitude can be calculated. Newton's Second Law of motion was used to estimate the impact force (F) from the product of the object's constant weight (mass, m) and its change of velocity over time (acceleration, a) (Eq. 1). In this experimental setup, the impact duration varies slightly with flow rates and type of obstruction. It is therefore considered as (t_i), accounting for the time from initial contact of the dowel with the structure until peak magnitude. The displacement parameter (Δx) was transformed to express the impact duration; a representative value can be calculated by considering the work and kinetic energy of the dowel (Eq. 2). Impact forces obtained from the sensor-tagged wooden dowel's acceleration data ($F_{\text{SmartWood}}$, Eq. 1), as well as from the average velocity estimates over the last meter before impact ($F_{\text{Work-Kinetic-Energy}}$, Eq. 2), were then compared to reference values from the Impulse-Momentum as well as Contact-Stiffness approach (Haehnel and Daly (2004):

$$F_{\text{SmartWood}} = m * a \ (N) \tag{1}$$

$$F_{\text{Work-Kinetic Energy}} * \Delta x = \frac{1}{2} * m * v^2 \ (J) \text{ with } \Delta x = \frac{v_0 + v_t}{2} * t \ (m) \tag{2}$$

Haehnel and Daly (2002) adapted the Impulse-Momentum approach, such as applied by FEMA (1995) and the U.S. Army Corps of Engineers (1995), which initially set the time of impact duration to a value of 1 s. This value, however, overestimates the stopping time, resulting in an underprediction of the maximum impact force. A 1-DoF model, as presented by Haehnel and Daly (2002), expresses the impact-impulse as a sinusoidal shape and predicts the maximum impact force using the LW momentum and the function of the impact duration ($\pi/2t_i$). This results in a relationship between impact force and sinusoidal shape, such as expressed in Eq. 3. Based on experiments, using prototype logs in a laboratory setup, Haehnel and Daly (2002) found a correlation between maximum impact force and momentum, showing a slope of 90.9 s^{-1}, which equals an impact duration of roughly 17 ms, following Eq. 4.

$$F_{\text{Impulse-Momentum}} = \frac{\pi}{2 \cdot t_i} \cdot v \cdot m \ (N) \tag{3}$$

$$F_{\text{IM,max}} = 90.9 \cdot v \cdot m \ (N) \text{ using } \frac{\pi}{2 \cdot t_i} = 90.9 \ s^{-1} \tag{4}$$

Furthermore, the Contact-Stiffness approach, initially introduced by AASHTO (1998), was adapted by Haehnel and Daly (2004) and uses a spring-mass system,

which requires the impact stiffness (k) between LW and in-stream structure. This 1-DoF model considers the in-stream structure to be rigid, as a spring-mass system is used, and predicts the maximum impact force using Eq. 5. Since the contact stiffness depends on the log weight and impact duration, obtained from the measured sensor data, the stiffness term is transformed to express the impact duration, which could then be applied in Eq. 6. The experiments were only focusing on straight impacts, which simplified the relationship by neglecting the term of the added mass coefficient, accounting for orientation with respect to acceleration direction (C), and the weight of the displaced fluid (m_f) (Eq. 7).

$$F_{\text{Contact-Stiffness}} = v \cdot \sqrt{k \cdot (m + C \cdot m_f)} \ (\text{N}) \tag{5}$$

$$t_{iCS} = \frac{\pi}{2} \cdot \sqrt{\frac{m}{k}} \ (s) \text{ equals}: \ k = \left(\frac{\pi}{2 \cdot t_i}\right)^2 \cdot m \ (\text{N} \cdot m^{-1}) \tag{6}$$

$$F_{\text{CS, max}} = v \cdot \sqrt{k \cdot m} \ (\text{N}) \tag{7}$$

3 Results

3.1 Impacts on a bridge pier

A total of 27 experiments out of 150 experiments, across the three flow rates of 10 (9), 35 (8) and 75 l s^{-1} (10), were considered successful, resulting in straight impacts upon the bridge pier structure (Fig. 3). Sensor data from the accelerometer revealed peak impact magnitudes between 699 and 3855 mg (Fig. 4), with impact duration ranging from 10 to 40 ms.

The average acceleration and impact duration for the 27 successful impacts were 2146 mg and 16.9 ms, respectively. Using Eq. 1, an average impact force of 1.05 N was calculated. The average impact force decreased with increasing flow rate. Flows of 10 l s^{-1} resulted in an average impact force of 1.21 N (average sensor data from accelerometer, 2476 mg), 35 l s^{-1} in 0.99 N (2012 mg), and 75 l s^{-1} in 0.96 N (1958 mg) (Figs. 5 and 6). The average impact durations for the three flow rates of 10, 35, and 75 l s^{-1} were 17.8, 15.0, and 17.5 ms.

Impact forces calculated based on the Work-Kinetic Energy approach required dowel velocity before impact, which was obtained from the video analysis. A minimum dowel velocity of 0.38 m s^{-1} and a maximum velocity of 1.50 m s^{-1} were recorded. The average dowel velocity, across all 27 experimental tests with straight impacts, was 0.94 m s^{-1}. At a flow rate of 10 l s^{-1}, the sensor-tagged wooden dowel traveled at an average velocity of 0.53 l s^{-1}. With increasing flow rate, the average flow velocity rose to 0.90 m s^{-1} (35 l s^{-1}) and 1.33 m s^{-1} (75 l s^{-1}). The Work-Kinetic Energy approach resulted in estimates of average impact force of 1.64 N (10 l s^{-1}), 3.45 N (35 l s^{-1}), and 4.61 N (75 l s^{-1}), with an overall average force of 3.27 N. An impact minimum of 0.95 N was calculated at the lowest flow rate. In contrast, a maximum of 7.50 N was recorded for the highest flow rate.

Using the Impulse-Momentum approach resulted in a further increase of the estimated impact force. The lowest flow rate resulted in an average impact force of 2.41 N,
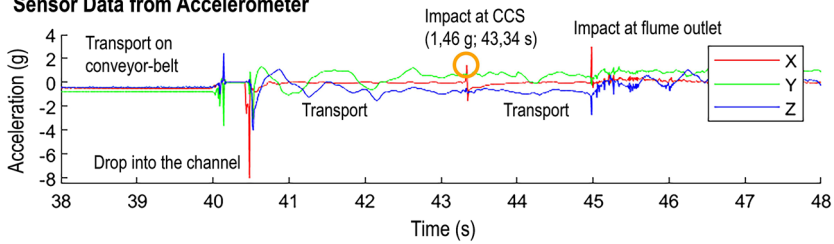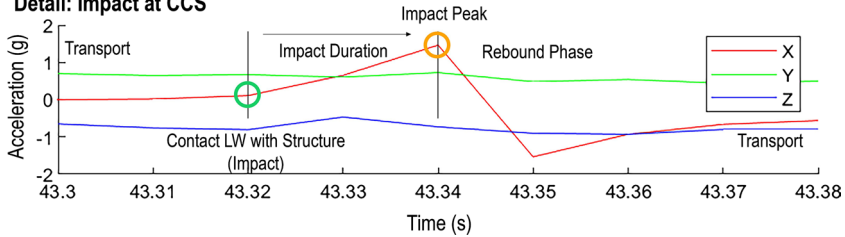
Fig. 4 Acquired sensor data from accelerometer for LW impact studies **a**. A high-resolution section of sensor data from the accelerometer **b**, displaying the time of first contact between LW and the in-stream structure (green circle), impact duration, and the maximum impact magnitude (impact peak, orange circle) measured as acceleration
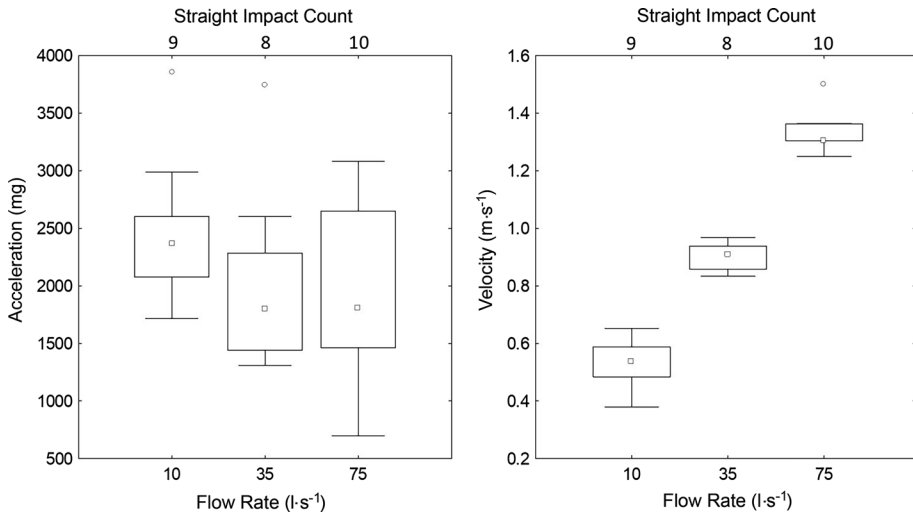

Fig. 5 Statistical evaluation of acceleration and dowel velocity data for each flow rate (FR) for the bridge pier configuration. Acceleration data show a descending tendency with increasing flow rate, while an increase in dowel velocity can be observed with rising flow rates. The whiskers represent the 10th and 90th percentiles, the box limits indicate the 25th and 75th percentiles and the square icon within the box marks the median

continuously increasing with increasing flow rate to 4.10 N and 6.02 N, respectively, with an overall average force across the 27 tests of 4.25 N. According to Eq. 4, the impact force increased linearly with the dowel velocity. Maximum observed impact forces were 2.96 N
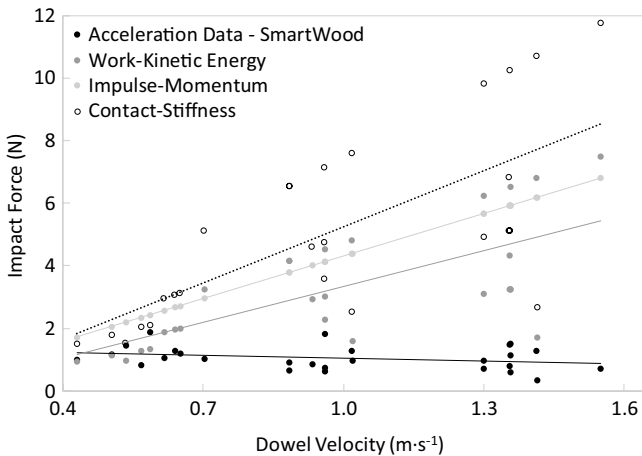
Fig. 6 LW impact forces on the bridge pier plotted against dowel velocity obtained from video analysis. Calculations from acceleration data indicate a decreasing trend of impact forces with increasing flow velocity (R^2 of 0.0756). Impact forces calculated using the Work-Kinetic Energy, Impulse-Momentum, and Contact-Stiffness approaches show an overall increasing trend of impact force with increasing flow velocity

for the lowest flow rate with a dowel velocity of 0.65 m s^{-1}, increasing to 4.40 N (0.97 m s^{-1}), and 6.81 N (1.50 m s^{-1}), respectively.

The Contact-Stiffness approach yielded results that are similar to the Impulse-Momentum approach. With increasing flow rate, the average impact force increased from 2.58 to 5.41 N, with the highest average impact force reaching 7.23 N for a flow rate of 75 l s^{-1}. The overall average force across the 27 tests was 5.14 N. For the lowest tested flow rate, the highest dowel velocity was 0.65 m s^{-1}, resulting in an estimated maximum impact force of 5.12 N. At 35 l s^{-1}, the dowel velocity increased to 0.97 m s^{-1}, with a resulting impact force of 7.60 N. Using the Contact-Stiffness approach, a maximum impact force of 11.78 N is obtained, with a corresponding maximum dowel velocity of 1.50 m s^{-1}.

3.2 Impacts on a LW retention structure

Experimental trials measuring impacts on a LW retention structure yielded a total of 123 successful runs (out of 150 experiments), comprising 40 successful impact tests with straight impact at the lowest flow rate, 44 at 35 l s^{-1}, and 39 at 75 l s^{-1}. The average acceleration measured by the sensor-tagged wooden dowel was 4189 mg; there was an increasing trend with increasing flow rates, namely: 3110 mg (10 l s^{-1}), 4633 mg (35 l s^{-1}), and 4793 mg (75 l s^{-1}) (Fig. 7). The mean dowel velocity in all experimental impact tests on the retention structure was 1.04 m s^{-1}, with a minimum of 0.22 m s^{-1} at 10 l s^{-1} and a maximum of 1.88 m s^{-1} at 75 l s^{-1} Dowel velocity increased with flow rate: 0.22–0.81 m s^{-1} at the lowest flow rate, 0.63–1.20 m s^{-1} at 35 l s^{-1}, and 0.91–1.88 m s^{-1} at the highest flow rate (Fig. 7). The average impact durations were measured as 14.1 ms (10 l s^{-1}), 15.0 ms (35 l s^{-1}), and 16.5 ms (75 l s^{-1}).

Overall, the maximum impact force measured via accelerometer varied between 0.41 N and 4.20 N, with an average of 2.06 N. The maximum impact forces increased with the flow rate from 1.53 to 2.27 N and eventually 2.35 N. Using the Work-Kinetic Energy approach, impact magnitudes ranged from 0.79 to 5.69 N with increasing flow rate. For
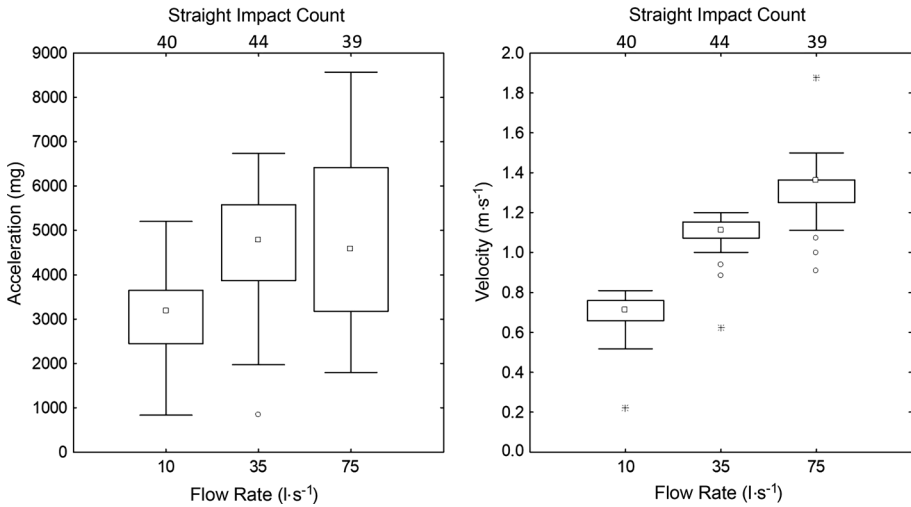
Fig. 7 Statistical evaluation of acceleration and dowel velocity data for each flow rate (FR) for experiments with the LW retention structure in place. An increasing trend for both acceleration as well as dowel velocity can be observed with increasing flow rate. The whiskers represent the 10th and 90th percentiles, the box limits indicate the 25th and 75th percentiles and the square icon within the box marks the median

all 123 impact experiments, the average impact force was 3.37 N. The mean values of the maximum impact force for increasing flow rate were 2.48 N, 3.64 N, and 3.99 N. The Impulse-Momentum approach resulted in an overall average impact force of 4.70 N, with 3.17 N ($10\,l\,s^{-1}$), 4.97 N ($35\,l\,s^{-1}$), and 5.98 N ($75\,l\,s^{-1}$), on average, for individual flow rates. Using the Contact-Stiffness approach, the overall average impact force was 5.30 N (123 experiments), with 3.89 N ($10\,l\,s^{-1}$), 5.72 N ($35\,l\,s^{-1}$), and 6.26 N ($75\,l\,s^{-1}$) on average for individual flow rates (Fig. 8).

4 Discussion

4.1 Impact force and impact duration

In the experimental setup, the impact duration (the time between the initial contact of dowel and structure until peak magnitude) varied between 10 and 40 ms across all flow rates and structures. The mean impact duration for impacts on the LW retention structure (15.2 ms) was slightly shorter than the stopping time of impacts on a bridge pier (16.9 ms). The measured impact durations in the present study, using an isolated sensor-unit, align with mean stopping times from LW impact studies found in the literature (e.g., 16.5 ms and 17 ms by Haehnel and Daly (2002) and 7–25 ms by Ikeno et al. (2016)), for similar log velocities. Generally, the present study affirms that movement analysis of logs from video footage is suitable for logs that are transported at the water surface, such as described by Alonso (2004). Yet, challenges arise due to the relatively low number of frames per second (30 fps), which is a common frame rate for video recordings. It has been shown that video recordings of 30 fps are sufficient to estimate the average log velocity over the last meter before impact, however, the frame rate is insufficient for estimating impact duration. Zhang et al. (2020) have recently shown that selecting an appropriate frame rate for camera-based
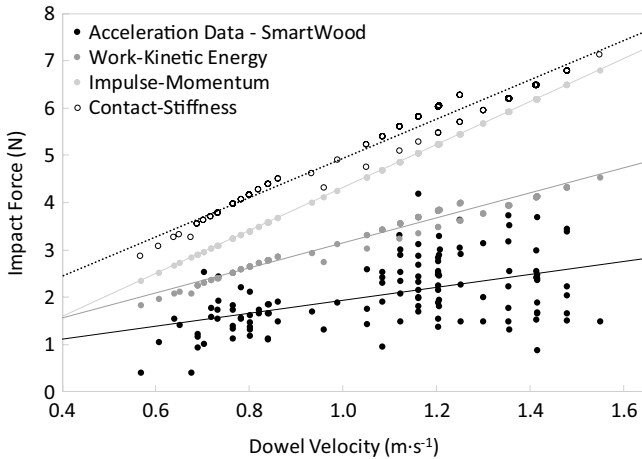
Fig. 8 LW impact forces on the retention structure compared to dowel velocity obtained from video analysis. All impact force calculation approaches show increased impact force with increased dowel velocity

velocity estimation is important. If the event is filmed at sufficiently high frequency, this can potentially determine the impact duration. Theoretically, a minimum frame rate of 120 fps is required to resolve impact periods of 16.6 ms or less, as previously observed by others (Haehnel and Daly 2002; Ikeno et al. 2016) and corroborated in the present study using an isolated sensor-unit.

This study confirms that impact duration significantly influences the maximum impact force. Stolle et al. (2019) evaluated the use of the rigid body model, the Contact-Stiffness approach, and a 2-DoF approach; all approaches overestimated the impact forces measured in their experiments, similar to present findings from experiments using high-resolution sensor data (Figs. 6 and 8). Deviations between theoretically estimated and precisely measured impact forces from the present study are summarized in Fig. 9. Here a similar magnitude of deviation (8-times overestimation) for bridge pier impacts, such as reported by Stolle et al. (2019), was observed. It is important to note that the different theoretical approaches yield somewhat more accurate estimates for the force on LW retention structures, overestimating the maximum impact force by a factor of less than three.

Given the form of the governing equations (Equations. 2–5, 7), log velocity is a sensitive variable for the assessment of impact forces. The application of an averaged log velocity may lead to a significant overestimation of the actual impact force. The theoretical approaches of Work-Kinetic Energy, Impulse-Momentum, and Contact-Stiffness all used the average log velocity, which is typically obtained over a certain distance before impact, similar to the method introduced by MacVicar and Piégay (2012). Log velocity estimates from video analysis may be of use for impact studies in homogenous hydraulic flow conditions that monitor conditions from the inertial frame of the impacted structure (Haehnel and Daly 2004; Ikeno et al. 2016). However, averaged velocity estimates from video analysis do not have the necessary temporal resolution and precision for the estimation of impact forces during floods in which turbulence, rapid changes in water surface elevation or flow deflections and other hydraulic effects (e.g., surface roller at bridge piers) dominate transport behavior and interactions. When using log velocity for impact studies, log velocity immediately before the initial contact with the structure is
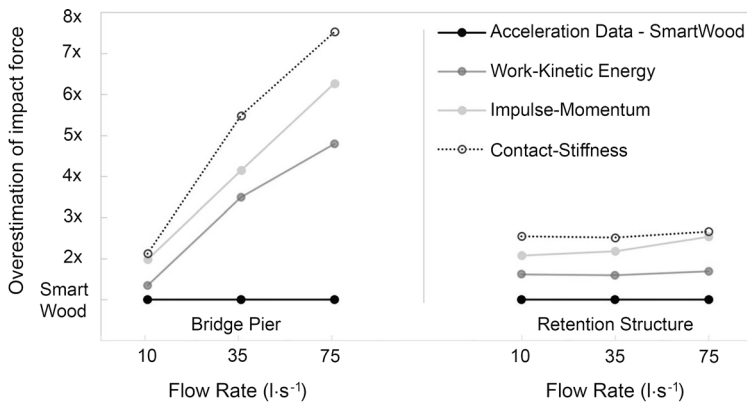
Fig. 9 Deviation from the maximum impact force (based on the measured acceleration data) for the Work-Kinetic Energy, Impulse-Momentum, and Contact-Stiffness approach, for both structures (bridge pier, LW retention structure) for varying flow rates

considered. This is difficult to determine using video footage due to rapidly changing flow conditions, as shown in the present study. For this reason, previous studies often resulted in an overprediction of impact forces (Stolle et al. 2019). This overprediction can be seen as a conservative safety factor at field-scale, acknowledging that there is no 'perfect' impact. However, local variations in flow hydraulics may also lead to log acceleration shortly before the collision, leading in turn to increased impact magnitudes.

The consideration of hydraulic effects is crucial for the assessment of LW impact forces. The surface roller effect generated in our physical model study (Fig. 10a) captures analogous flow conditions observed in prototype environments (Fig. 10b) and was shown to significantly affect the impact magnitude of LW collision, relative to the traditionally applied impact force estimation approaches. At higher flow rates and flow velocities the leading end of the LW was diverted, and the sensor-tagged wooden dowel rotated as it struck the bridge pier (in-stream structure), thus attenuating the impact. The effect of the surface roller resulted in a longer impact duration, leading to a reduced acceleration force, as determined from the sensor, and consequently lower impact forces at higher flow rates (Fig. 6). Using the Work-Kinetic Energy approach, with the dowel velocity over the last meter before impact, will not account for the surface roller effect, leading to overestimation of impact. The presence of the LW retention structure, on the other hand, showed negligible effects on flow hydraulics and resulted in a rising trend of impact force with increasing flow rate (Fig. 8), such as previously shown for increasing flow velocities (Haehnel and Daly 2004).

This study applied measurements of impact duration (stopping time) to calculate impact forces from LW collisions. We found a strong tendency toward overestimation of the velocity component contributing to the impact force, relative to measurements from an isolated acceleration sensor attached to a wooden dowel. Stopping distance and contact stiffness are independent parameters, yet are strongly dependent on a time component. While stopping distance depends on impact duration and LW velocity, impact duration can also be expressed as a function of LW weight and effective contact stiffness (Haehnel and Daly 2004; Stolle et al. 2018).
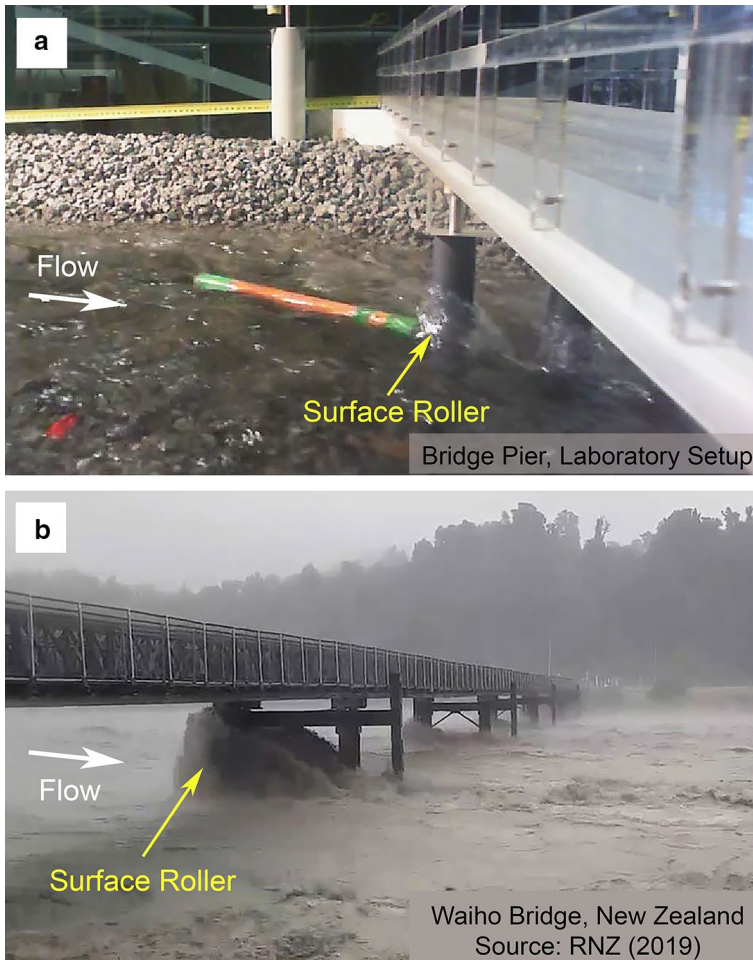
Fig. 10 **a** The surface roller effect generated in the scaled laboratory environment, and **b** during a flood on the Waiho River at the State Highway 6 Bridge on New Zealand's West Coast on 26 Mar 2019. RNZ (2019) (**b**)

The maximum measured impact force (4.2 N; Fig. 8) is equivalent to a maximum field-scale impact force of $14.2 \; 10^3$ N (Froude similarity), with is consistent with the relatively large range (10^2 and 10^4 N) of impact magnitudes found in the literature (Haehnel and Daly 2004; Ko et al. 2015; Ikeno et al. 2016; Stolle et al. 2018). Dowel velocities in this physical model study ranged up to 1.5 m s^{-1}, representing a travel velocity of roughly 5.8 m s^{-1} in a prototype environment. Flow velocities at this high range align with observations (2.5–8 m s^{-1}) from previous studies (Smith 1994; Kreibich et al. 2009), and may show significant effects on flow hydraulics around in-stream structures (Fig. 10b).

4.2 Transport orientation

Not all experimental runs resulted in straight impacts on the in-stream structures. For the experiments using a channel-spanning LW retention structure, 123 out of 150 tests were classified as straight impacts, meaning that 82% of the total experiments exhibited generally parallel alignment of the wooden dowel with the flow at the CCS. Experiments conducted at the lowest (10 l s^{-1}) and highest (75 l s^{-1}) flow rate revealed almost identical (80% and 78%) probabilities for straight LW transport at the CCS, while the middle flow rate (35 l s^{-1}) had a slightly higher probability (88%) of parallel LW alignment with the flow. It has been noted that the middle flow rate exhibited the 'smoothest' water surface, at moderate water depths and flow velocities. This is in contrast to the lowest water level (10 l s^{-1}), where flow deflections arose from interactions with the rough channel elements. The highest flow rate (75 l s^{-1}) showed more turbulent flow conditions and higher water levels. For the experiments using the bridge pier, on average, only 18% of the tests produced straight impacts on the bridge pier. Every fifth log not only moved parallel with the flow, but also exactly in the centerline of the channel when approaching the CCS (Figs. 1 and 3). The lower probability of straight impacts onto the bridge pier is a consequence of the reduced cross-sectional area of the pier structure, with regards to a channel-crossing retention structure. Transport of LW in parallel with the flow is commonly observed and consistent with findings in previous LW research (Braudrick and Grant 2001; Chen et al. 2019), yet the present study revealed that transport orientation strongly depends on prevailing hydraulic flow conditions (e.g. water depth, flow velocity, turbulences) and uniformity of the channel (e.g. with/without individual rough channel elements and in-stream structures). The present study focused on individual log transport, which is expected to show different orientation and movement dynamics than congested transport behavior (Ruiz-Villanueva et al. 2019).

5 Conclusions and outlook

LW impact forces, arising from collisions between wood in transit and in-stream structures have been quantified in detail, using a novel methodology. Although LW impacts are not a natural hazard on their own, destructive impacts in fluvial and coastal environments typically occur during floods, debris flows, landslides or tsunamis, and are extremely difficult to capture due to the turbulent and hostile environment and rapidly changing conditions. Thus, an innovative sensor-unit, implanted into scaled logs, was employed for measuring impact forces and impact duration in a physical model study. The observed transport behavior confirmed that the sensor-tagged logs were suited for the study.

Dowel acceleration decreased with increasing flow rate and magnified hydraulic effects at the bridge pier, while impact forces increased with increasing flow rate at the retention structure. Impact duration represents a crucial parameter for the determination of impact forces and was measured in the range from 10 to 40 ms for both tested structures. Shorter impact duration typically results in higher impact forces. However, impact duration is also subject to physical parameters, such as log stiffness and rigidity of the hydraulic structure. While well preserved (fresh) logs at field scale may show a higher stiffness than logs in an advanced decay stage, impact duration and damage potential

upon impact may vary significantly. The impact delivered by more complex tree forms, for instance, with branches and root wad attached, may tend to have longer impact durations and damping of impact forces.

At higher flow rates, conventionally applied estimation methods tend to overpredict the actual impact force due to the use of an averaged log velocity, rather than the actual log velocity at initial contact with the structure. Hydraulic effects (e.g., surface roller, flow deviation, eddies) significantly affect log velocity, stopping time, and impact magnitude, and potentially lead to an LW acceleration before the impact, causing more severe damage to the structure. However, hydraulic effects are not considered in conventional impact force estimates, thus diminishing the accuracy of predictions of impact force during flood or mass flow conditions. Precise estimation of LW impact forces requires accurate capture of log acceleration and impact in the scant few milliseconds of collision time.

The present study contributes to a better understanding of impact forces arising from LW in transit. It points out the importance of considering structural design (e.g., shape and geometry of in-stream structures) and prevailing flow hydraulics for the determination of impact magnitudes. Although impact forces of LW are generally relatively small with respect to the mass and stiffness of the structure, destruction from LW impacts during in flood and torrents is often observed, thus posing a risk to critical infrastructure and buildings nearby. Ultimately, there is a strong imperative to improve our knowledge of load dynamics from LW in transit, both in laboratory and field experiments. Remotely sensed, high-resolution data will play a key role in future LW research. This could also play a role in more detailed and sophisticated monitoring of semi-congested, congested. and hyper-congested transport behavior (Ruiz-Villanueva et al. 2019). Furthermore, it could shed light on the movements of more complex LW components, taking account of variable wood density and geometry, including branches and root wads. Furthermore, various obstruction designs (e.g., bridge pier shape, inclined retention structures, engineered log jams) may be considered for LW impact studies. An advanced understanding of impact forces will generate better assessment of the vulnerability of existing structures and will help in the design of flood-resilient structures to maintain safety in and around LW-prone fluvial systems.

Data availability Data that support the findings of this study are available upon request from the authors. The data are not publicly available due to confidential information, which may be subject to further publications.

Declarations

Conflict of interest The authors declare that they have no known competing financial interests or personal relationships that could have appeared to influence the work reported in this paper.

References

AASHTO (1998) LRFD bridge design specifications. Am as State Highw Transp off 2 Haehnel Daly 2004:26–27. https://doi.org/10.1061/~ASCE!0733-9429~2004!130:2~112!

Abbe TB, Montgomery DR (2003) Patterns and processes of wood debris accumulation in the Queets river basin. Wash Geomorphol 51(1–3):81–107. https://doi.org/10.1016/s0169-555x(02)00326-4

Ahmad N, Ghazilla RAR, Khairi NM, Kasi V (2013) Reviews on various inertial measurement unit (IMU) sensor applications. Int J Signal Process Syst. https://doi.org/10.12720/ijsps.1.2.256-262

Aldoumani N, Meydan T, Dillingham CM, Erichsen JT (2016) Enhanced tracking system based on micro inertial measurements unit to measure sensorimotor responses in pigeons. IEEE Sens J 16(24):8847–8853. https://doi.org/10.1109/jsen.2016.2586540

Alonso CV (2004) Transport mechanics of stream-borne logs. Water Sci Appl 8:59–69. https://doi.org/10.1029/008WSA05

Asghar M, Pasha GA, Ghani U, Iqbal S, Jameel MS (2020) Investigating multiple debris impact load and role of vegetation in protection of house model during floods. 2nd conference on sustainability in civil engineering, 7. https://csce.cust.edu.pk/archive/20-411.pdf

Bein P (1990) Methodology for assessment of vessel impact engery on bridge piers and spans. Transp Res Rec 1275. http://onlinepubs.trb.org/Onlinepubs/trr/1990/1275/1275-012.pdf

Braudrick CA, Grant GE (2000) When do logs move in rivers? Water Resour Res 36(2):571–583. https://doi.org/10.1029/1999wr900290

Braudrick CA, Grant GE (2001) Transport and deposition of large woody debris in streams: a flume experiment. Geomorphology 41(4):263–283. https://doi.org/10.1016/S0169-555x(01)00058-7

Braudrick CA, Grant GE, Ishikawa Y, Ikeda H (1997) Dynamics of wood transport in streams-a flume experiment. Earth Surf Process Landf 22(7):669–683. https://doi.org/10.1002/(SICI)1096-9837(199707)22:7%3c669::AID-ESP740%3e3.0.CO;2-L

Cabral VC, Reis FAGV, D'Affonseca FM, Lucía A, Dos Santos Corrêa CV, Veloso V, Gramani MF, Ogura AT, Lazaretti AF, Vemado F, Pereira Filho AJ, Dos Santos CC, Lopes ESS, Rabaco LMR, Do Carmo Giordano L, Zarfl C (2021) Characterization of a landslide-triggered debris flow at a rainforest-covered mountain region in Brazil. Nat Hazards 108(3):3021–3043. https://doi.org/10.1007/s11069-021-04811-9

Cave M, Davies N, Langford J (2017) Cyclone cook slash investigation 2017 report. Gisborne Dist Counc Land Soil Environ Serv Prot, 121. https://www.gdc.govt.nz/__data/assets/pdf_file/0013/10408/cyclone-cook-slash-investigation-2017-report.pdf

Caviezel A, Demmel SE, Ringenbach A, Bühler Y, Lu G, Christen M, Dinneen CE, Eberhard LA, von Rickenbach D, Bartelt P (2019) Reconstruction of four-dimensional rockfall trajectories using remote sensing and rock-based accelerometers and gyroscopes. Earth Surf Dyn 7(1):199–210. https://doi.org/10.5194/esurf-7-199-2019

Chen S-C, Tfwala SS, Wang C-R, Kuo Y-M, Chao Y-C (2019) Incipient motion of large wood in river channels considering log density and orientation. J Hydraul Res 58(3):489–502. https://doi.org/10.1080/00221686.2019.1625816

Chuang W-L, Chang K-A, Kaihatu J, Cienfuegos R, Mokrani C (2020) Experimental study of force, pressure, and fluid velocity on a simplified coastal building under tsunami bore impact. Nat Hazards 103(1):1093–1120. https://doi.org/10.1007/s11069-020-04027-3

Chung CH, Lee J, Gil JH (2013) Structural performance evaluation of a precast prefabricated bridge column under vehicle impact loading. Struct Infrastruct Eng 10(6):777–791. https://doi.org/10.1080/15732479.2013.767841

Codecian co ltd (2007) Pelscope: a tool to check/measure image quality. http://www.codecian.com/index.html

Elliot RC, Froehlich DC, Macarthur RC (2012) Calculating the potential effects of large woody debris accumulations on backwater, scour, and hydrodynamic loads. World Environ Water Resour Congr 2012:1213–1222. https://doi.org/10.1061/9780784412312.123

El-Tawil S, Severino E, Fonseca P (2005) Vehicle collision with bridge piers. J Bridge Eng. https://doi.org/10.1061/(ASCE)1084-0702(2005)10:3(345)

Eu S, Im S, Kim D (2019) Development of debris flow impact force models based on flume experiments for design criteria of soil erosion control dam. Adv Civ Eng 2019:1–8. https://doi.org/10.1155/2019/3567374

Fan W, Yuan WC (2014) A simple procedure for determination of the dynamic ship-impact load on bridge structures. WIT Trans Built Environ 141:73–85. https://doi.org/10.2495/susi140071

Fausch KD, Northcote TG (1992) Large woody debris and salmonid habitat in a small coastal British Columbia stream. Can J Fish Aquat Sci 49:682–693

Fema F (1995) Engineering principles and practices for retrofitting flood prone residential buildings. Federal Emergency Management Agency, Report No. 259

Fischer C, Sukumar PT, Hazas M (2013) Tutorial: implementing a pedestrian tracker using inertial sensors. IEEE Pervasive Comput 12(2):17–27. https://doi.org/10.1109/Mprv.2012.16

Gasser E, Schwarz M, Simon A, Perona P, Phillips C, Hübl J, Dorren L (2019) A review of modeling the effects of vegetation on large wood recruitment processes in mountain catchments. Earth Sci Rev 194:350–373. https://doi.org/10.1016/j.earscirev.2019.04.013

Ghaffarian H, Piégay H, Lopez D, Rivière N, Macvicar B, Antonio A, Mignot E (2020) Video-monitoring of wood discharge: first inter-basin comparison and recommendations to install video cameras. Earth Surf Process Landf 45(10):2219–2234. https://doi.org/10.1002/esp.4875

Gilbert GK, Murphy EC (1914) The Transportation of debris by running water. US Geol Surv Prof Pap 86:1–263. https://doi.org/10.3133/pp86

Gippel C (1995) Environmental hydraulics of large woody debris in streams and rivers. J Environ Eng 121(5):388–395

Goseberg N, Nistor I, Mikami T, Shibayama T, Asce M, Stolle J (2016) Nonintrusive spatiotemporal smart debris tracking in turbulent flows with application to debris-laden tsunami inundation. J Hydraul Eng 142(12):17

Gschnitzer T, Gems B, Mazzorana B, Aufleger M (2017) Towards a robust assessment of bridge clogging processes in flood risk management. Geomorphology 279:128–140. https://doi.org/10.1016/j.geomorph.2016.11.002

Gurnell AM, Piegay H, Swanson FJ, Gregory SV (2002) Large wood and fluvial processes. Freshw Biol 47:601–619

Haehnel RB, Daly SF (2002) Maximum impact force of woody debris on floodplain structures. US Army Corps Eng 53. https://apps.dtic.mil/sti/pdfs/ADA398916.pdf

Haehnel RB, Daly SF (2004) Maximum impact force of woody debris on floodplain structures. J Hydraul Eng 130(2):112–120. https://doi.org/10.1061//ASCE/0733-9429/2004/130:2/112

Ikeno M, Takabatake D, Kihara N, Kaida H, Miyagawa Y, Shibayama A (2016) Improvement of collision force formula for woody debris by airborne and hydraulic experiments. Coast Eng 58(4):23. https://doi.org/10.1142/s0578563416400222

Iroumé A, Mao L, Andreoli A, Ulloa H, Ardiles MP (2015) Large wood mobility processes in low-order Chilean river channels. Geomorphology 228:681–693. https://doi.org/10.1016/j.geomorph.2014.10.025

Jakob M, Stein D, Ulmi M (2011) Vulnerability of buildings to debris flow impact. Nat Hazards 60(2):241–261. https://doi.org/10.1007/s11069-011-0007-2

Kamaitis Z (1995) Vehicle accidental impacts on bridges. Statyba 3(12):20–27. https://doi.org/10.1080/13921525.1997.10531363

Keller E, Macdonald A, Tally T, Merrit NJ (1979) Effects of large organic debris on channel morphology and sediment storage in selcted tributaries of redwood creek, northwestern California-geomorphic processes and aquatic habitat in the redwood creek basin, northwestern California. US Geol Surv Prof Pap 32:1454

Ko HTS, Cox DT, Riggs HR, Naito CJ (2015) Hydraulic experiments on impact forces from Tsunami-driven debris. J Waterw Port Coast Ocean Eng 141(3):04014043

Kreibich H, Piroth K, Seifert I, Maiwald H, Kunert U, Schwarz J, Merz B, Thieken AH (2009) Is flow velocity a significant parameter in flood damage modelling? Nat Hazards Earth Syst Sci 9:1678–1692

Liang D, Jian W, Shao S, Chen R, Yang K (2017) Incompressible SPH simulation of solitary wave interaction with movable seawalls. J Fluids Struct 69:72–88. https://doi.org/10.1016/j.jfluidstructs.2016.11.015

Macvicar B, Piégay H (2012) Implementation and validation of video monitoring for wood budgeting in a wandering piedmont river, the Ain River (France). Earth Surf Process Landf 37(12):1272–1289. https://doi.org/10.1002/esp.3240

Macvicar BJ, Piegay H, Henderson A, Comiti F, Oberlin C, Pecorari E (2009) Quantifying the temporal dynamics of wood in large rivers: field trials of wood surveying, dating, tracking, and monitoring techniques. Earth Surf Process Landf 34(15):2031–2046. https://doi.org/10.1002/esp.1888

Martin DJ, Harden CP, Tran L, Opavlowsky RT (2018) Investigating patterns of in-channel wood deposition locations in a low gradient, variably-confined alluvial river system. Prog Phys Geogr 42(2):139–161. https://doi.org/10.1177/0309133318759613

Marvi MT (2020) A review of flood damage analysis for a building structure and contents. Nat Hazards 102(3):967–995. https://doi.org/10.1007/s11069-020-03941-w

Mazzorana B, Fuchs S (2010) Fuzzy formative scenario analysis for woody material transport related risks in mountain torrents. Environ Model Softw 25(10):1208–1224. https://doi.org/10.1016/j.envsoft.2010.03.030

NAASRA (1990) Highway Bridge Design Specification. National Association of Australian State Road Authorities. Our literature review revealed that the relevant version of the book by NAASRA has been published in 1970 with the proper reference: NAASRA (1970) Highway Bridge Design Specification. National Association of Australian State Road Authorities. 4th Edn

Nadal NC, Zapata RE, Pagán I, López R, Agudelo J (2010) Building damage due to riverine and coastal floods. J Water Resour Plan Manag 136(3):327–336. https://doi.org/10.1061/(asce)wr.1943-5452.0000036

Nakamura F, Swanson FJ (1994) Distribution of coarse woody debris in a mountain stream, western cascade range. Oregon Can J for Res 24(12):2395–2403. https://doi.org/10.1139/x94-309

Nam D, Kim M-I, Kang D, Kim B (2019) Debris flow damage assessment by considering debris flow direction and direction angle of structure in South Korea. Water. https://doi.org/10.3390/w11020328

Phillips C, Marden M, Basher LR (2018) Geomorphology and forest management in New Zealand's erodible steeplands: an overview. Geomorphology 307:107–121. https://doi.org/10.1016/j.geomorph.2017.07.031

Piran Aghl P, Naito CJ, Riggs HR (2014) Full-scale experimental study of impact demands resulting from high mass low velocity debris. J Struct Eng 140(5):04014006. https://doi.org/10.1061/(asce)st.1943-541x.0000948

Ravazzolo D, Mao L, Picco L, Lenzi MA (2015) Tracking log displacement during floods in the Tagliamento River using RFID and GPS tracker devices. Geomorphology 228:226–233. https://doi.org/10.1016/j.geomorph.2014.09.012

Ravazzolo D, Mao L, Mazzorana B, Ruiz-Villanueva V (2017) Brief communication: the curious case of the large wood-laden flow event in the Pocuro stream (Chile). Nat Hazards Earth Syst Sci 17(11):2053–2058. https://doi.org/10.5194/nhess-2017-154

Riggs HR, Cox DT, Naito CJ, Kobayashi MH, Aghl PP, Ko HTS, Khowitar E (2013) Water-driven debris impact forces on structures: experimental and theoretical program. In: Proceedings of the ASME 32nd international conference on ocean, offshore and arctic engineering, 1. https://doi.org/10.1115/omae2013-11128

Ruiz-Villanueva V, Piegay H, Gurnell AA, Marston RA, Stoffel M (2016) Recent advances quantifying the large wood dynamics in river basins: new methods and remaining challenges. Rev Geophys 54(3):611–652. https://doi.org/10.1002/2015rg000514

Ruiz-Villanueva V, Mazzorana B, Bladé E, Bürkli L, Iribarren-Anacona P, Mao L, Nakamura F, Ravazzolo D, Rickenmann D, Sanz-Ramos M, Stoffel M, Wohl E (2019) Characterization of wood-laden flows in rivers. Earth Surf Process Landf 44:1694–1709. https://doi.org/10.1002/esp.4603

Rusyda MI, Hashimoto H, Ikematsu S (2014) Log jam formation by an obstruction in a river. River Flow 2014:717–724

Schenk ER, Moulin B, Hupp CR, Richter JM (2014) Large wood budget and transport dynamics on a large river using radio telemetry. Earth Surf Process Landf 39(4):487–498. https://doi.org/10.1002/esp.3463

Sha YY, Hao H (2013) Numerical simulation of barge impact on a continuous girder bridge and bridge damage detection. Int J Prot Struct 4(1):79–96. https://doi.org/10.1260/2041-4196.4.1.79

Shields FD, Alonso CV (2012) Assessment of flow forces on large wood in rivers. Water Resour Res. https://doi.org/10.1029/2011wr011547

Smith DI (1994) Flood damage estimation-a review of urban stage-damage curves and loss functions. Water SA 20(3):6

Sodhi DS, Haehnel RB (2003) Crushing ice forces on structures. J Cold Reg Eng 17(4):153–170. https://doi.org/10.1061/(asce)0887-381x(2003)17:4(153)

Spreitzer G, Gibson J, Tang M, Tunnicliffe J, Friedrich H (2019) Smart wood: laboratory experiments for assessing the effectiveness of smart sensors for monitoring large wood movement behaviour. CATENA. https://doi.org/10.1016/j.catena.2019.104145

Stolle J, Derschum C, Goseberg N, Nistor I, Petriu E (2018) Debris impact under extreme hydrodynamic conditions part 2: impact force responses for non-rigid debris collisions. Coast Eng 141:107–118. https://doi.org/10.1016/j.coastaleng.2018.09.004

Stolle J, Goseberg N, Nistor I, Petriu E (2019) Debris impact forces on flexible structures in extreme hydrodynamic conditions. J Fluids Struct 84:391–407. https://doi.org/10.1016/j.jfluidstructs.2018.11.009

Stolle J, Nistor I, Goseberg N, Petriu E (2020) Multiple debris impact loads in extreme hydrodynamic conditions. J Waterw Port Coast Ocean Eng. https://doi.org/10.1061/(asce)ww.1943-5460.0000546

Sturm M, Gems B, Keller F, Mazzorana B, Fuchs S, Papathoma-Köhle M, Aufleger M (2018) Experimental analyses of impact forces on buildings exposed to fluvial hazards. J Hydrol 565:1–13. https://doi.org/10.1016/j.jhydrol.2018.07.070

US Army (1995) Corps of engineers. Flood-proofing regulations. Engineering Pamphlet 1165-2-314, Washington, DC. https://www.publications.usace.army.mil/Portals/76/Publications/EngineerPamphlets/EP_1165-2-314.pdf

Wohl E, Jaeger K (2009) A conceptual model for the longitudinal distribution of wood in mountain streams. Earth Surf Process Landf 34(3):329–344. https://doi.org/10.1002/esp.1722

Wohl E, Bledsoe BP, Fausch KD, Kramer N, Bestgen KR, Gooseff MN (2016) Management of large wood in streams: an overview and proposed framework for hazard evaluation. J Am Water Resour as 52(2):315–335. https://doi.org/10.1111/1752-1688.12388

Worsey MT, Espinosa HG, Shepherd JB, Thiel DV (2019) Inertial sensors for performance analysis in combat sports: a systematic review. Sports (basel). https://doi.org/10.3390/sports7010028

Wyżga B, Mikuś P, Zawiejska J, Ruiz-Villanueva V, Kaczka RJ, Czech W (2017) Log transport and deposition in incised, channelized, and multithread reaches of a wide mountain river: tracking experiment during a 20-year flood. Geomorphology 279:98–111. https://doi.org/10.1016/j.geomorph.2016.09.019

Xu T, Sheng X, Zhang T, Liu H, Liang X, Ding A (2018) Development and validation of dummies and human models used in crash test. Appl Bionics Biomech 2018:3832850. https://doi.org/10.1155/2018/3832850

Zhang Z, Ghaffarian H, Macvicar B, Vaudor L, Antonio A, Michel K, Piegay H (2020) Video monitoring of in-channel wood: from flux characterization and prediction to recommendations to equip stations. HAL HAL Id: hal-03027976, 1–49. https://hal.archives-ouvertes.fr/hal-03027976/document

Zhou D, Li R, Wang J, Guo C (2017) Study on impact behavior and impact force of bridge pier subjected to vehicle collision. Shock Vib 2017:1–12. https://doi.org/10.1155/2017/7085392

Zhou X, Gao Y, Huang F, Zhang G (2019) A study on the collision force of reinforced concrete piers under cumulative ship collision. Adv Mech Eng 11(3):168781401983507. https://doi.org/10.1177/1687814019835071

Authors and Affiliations

Gabriel Spreitzer[1,2] · **Diego Ravazzolo[2,3]** · **Jon Tunnicliffe[4]** · **Heide Friedrich[2]**

Diego Ravazzolo
d.ravazzolo@uib.es

Jon Tunnicliffe
j.tunnicliffe@auckland.ac.nz

Heide Friedrich
h.friedrich@auckland.ac.nz

[1]　Laboratory of Hydraulics, Hydrology and Glaciology (VAW), ETH Zürich, 8093 Zurich, Switzerland

[2]　Department of Civil and Environmental Engineering, University of Auckland, Auckland 1010, New Zealand

[3]　Mediterranean Ecogeomorphological and Hydrological Connectivity Research Team, Department

of Geography, University of the Balearic Islands, 07122 Palma, Balearic Islands, Spain

4　　School of Environment, University of Auckland, Auckland 1010, New Zealand